

# Measurement of muonium emission from silica aerogel

P. Bakule<sup>9</sup>, G.A. Beer<sup>3</sup>, D. Contreras<sup>10</sup>, M. Esashi<sup>1</sup>, Y. Fujiwara<sup>8,5</sup>, Y. Fukao<sup>7</sup>, S. Hirota<sup>7,5</sup>, H. Iinuma<sup>7</sup>, K. Ishida<sup>8</sup>, M. Iwasaki<sup>8</sup>, T. Kakurai<sup>8,5</sup>, S. Kanda<sup>8,5</sup>, H. Kawai<sup>4</sup>, N. Kawamura<sup>7</sup>, G.M. Marshall<sup>10</sup>, H. Masuda<sup>2</sup>, Y. Matsuda<sup>6</sup>, T. Mibe<sup>7</sup>, Y. Miyake<sup>7</sup>, S. Okada<sup>8</sup>, K. Olchanski<sup>10</sup>, A. Olin<sup>10,3</sup>, H. Onishi<sup>8</sup>, N. Saito<sup>7,5</sup>, K. Shimomura<sup>7</sup>, P. Strasser<sup>7</sup>, M. Tabata<sup>4</sup>, D. Tomono<sup>8,†</sup>, K. Ueno<sup>7</sup>, K. Yokoyama<sup>8,‡</sup>, S. Yoshida<sup>1</sup>

<sup>1</sup>*Advanced Institute for Materials Research, Tohoku University, Sendai 980-8578, Japan*

<sup>2</sup>*Division of Applied Chemistry, Tokyo Metropolitan University, Tokyo, 192-0397, Japan*

<sup>3</sup>*Department of Physics and Astronomy, University of Victoria, Victoria BC V8W 3P6, Canada*

<sup>4</sup>*Department of Physics, Chiba University, Chiba 263-8522, Japan*

<sup>5</sup>*Department of Physics, The University of Tokyo, Tokyo, 113-0033, Japan*

<sup>6</sup>*Graduate School of Arts and Sciences, The University of Tokyo, Tokyo, 153-8902, Japan*

<sup>7</sup>*High Energy Accelerator Research Organization (KEK), Ibaraki, 305-0801, Japan*

<sup>8</sup>*RIKEN Nishina Center, RIKEN, Saitama, 351-0198, Japan*

<sup>9</sup>*RIKENRAL Muon Facility, Rutherford Appleton Laboratory, Harwell Oxford, Didcot, Oxfordshire, OX11 0QX, UK*

<sup>10</sup>*TRIUMF, Vancouver, BC, V6T 2A3, Canada*

.....  
Emission of muonium ( $\mu^+e^-$ ) atoms from silica aerogel into vacuum was observed. Characteristics of muonium emission were established from silica aerogel samples with densities in the range from 29 mg cm<sup>-3</sup> to 178 mg cm<sup>-3</sup>. Spectra of muonium decay times correlated with distances from the aerogel surfaces, which are sensitive to the speed distributions, follow general features expected from a diffusion process, while small deviations from a simple room-temperature thermal diffusion model are identified. The parameters of the diffusion process are deduced from the observed yields.  
.....

Subject Index      C31, G04

## 1. Introduction

A new experiment has been proposed at J-PARC [1] to measure the anomalous magnetic moment  $a_\mu = (g-2)_\mu/2$  of the muon. There exists a discrepancy of about  $3.5\sigma$  between the best existing measurement (0.54 ppm) [2] from the Brookhaven experiment (E821) and the best theoretical estimates [3, 4]. If the difference persists with higher precision experiments and theoretical calculations, it signals physics beyond the Standard Model. The Brookhaven method will be used in a similar improved experiment at Fermilab, but the J-PARC approach

<sup>†</sup>Present Address: School of Physics and Astronomy, Queen Mary University of London, Mile End Road, London E1 4NS, UK

<sup>‡</sup>Present Address: Dept. of Physics, Kyoto University, Kyoto, Japan

---

is quite different, and would be limited by much different systematic uncertainties. The J-PARC experiment relies on the acceleration of muons from essentially thermal energies, in order to limit transverse momentum components and to enable their eventual injection into a small storage device with a high-precision magnetic field. This requirement translates into the need for an ultra-slow muon source.

The most promising method to create an ion source for ultra-slow muons is from laser ionization of thermal muonium in vacuum. Muonium is the atomic bound state consisting of a positive muon and an electron ( $\mu^+e^-$  or Mu). It is chemically similar to a hydrogen atom, but as an antilepton-lepton bound state it has aspects in common also with positronium ( $e^+e^-$  or Ps). Muonium production occurs following thermalization of a positive muon beam in a variety of gases, liquids, and solids. Observation is typically signified by the distinctive frequency of muonium hyperfine transitions in weak transverse magnetic fields (1.4 MHz at  $10^{-4}$  T) that is observed in the 2.2  $\mu$ s decay time distribution of positrons following parity-violating polarized  $\mu^+ \rightarrow e^+\nu_e\bar{\nu}_\mu$  decays [5].

Fundamental interactions of muonium in vacuum have been investigated in several experiments such as searches for conversion of muonium to antimuonium ( $\mu^-e^+$ ) [6] and the precise measurement of the 1S-2S energy interval in Mu [7, 8]. Both required Mu at low (near thermal) energies in an environment free of other interactions, i.e., isolated in a vacuum. A key to their success was the development of techniques to produce Mu in a silicon dioxide (silica) powder that subsequently emits it into a vacuum [9–11].

Motivated by the extremely important  $(g-2)_\mu$  experiment, and by its need for a reliable, intense, ultra-slow muon source, we have undertaken systematic investigations of muonium emission into vacuum from potential target materials. The silica powder of the original method presented stability and handling problems, and was considered incompatible with the high precision requirements of  $(g-2)_\mu$ . Silica aerogel was identified as a promising alternative, producing polarized muonium with reasonably high probability from stopping muon beams, and also showing evidence of muonium emission into vacuum. Unlike powder, it is self-supporting, stable, and can be made in various sizes, shapes, and densities. This paper presents the results of our measurements of muonium behavior in a selection of high quality silica aerogel samples.

## 2. Aerogel samples

Four separate silica aerogel samples were investigated. All were fabricated at Chiba University with the same method used for high quality Cerenkov detector materials [12]. Surfaces of all samples were prepared using a process developed to make them hydrophobic, in order to limit absorption of water following the supercritical drying of the aerogels. The samples were manufactured in slabs of  $100 \times 100$  mm<sup>2</sup>, but were cut to obtain a muon stopping target of  $30 \times 40$  mm<sup>2</sup>, only slightly larger than the muon beam transverse dimensions. The samples were prepared with different densities of 29, 47, 97, and 178 mgcm<sup>-3</sup>, and with corresponding different thicknesses of 6.9, 4.8, 2.2, and 2.0 mm respectively. We wished to investigate the dependence of muonium emission on density in the context of our diffusion model. Higher density targets would provide higher proportions of muons stopping near the surface of the target, thus potentially leading to higher probability of muonium emission from that surface. The reduction of thickness with higher density reduced differences in

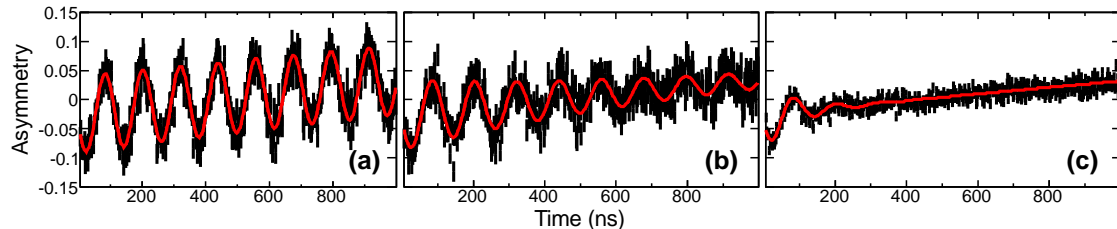


**Fig. 1** Muonium spin rotation asymmetry distributions and fits. The muon exponential decay time dependence has been removed. The muonium signal relaxation rate is proportional to the concentration of oxygen in the aerogel environment: (a) vacuum, (b)  $0.50(1) \times 10^{16} \text{ mol cm}^{-3}$ , and (c)  $4.57(3) \times 10^{16} \text{ mol cm}^{-3}$ .

target mass and consequently reduced possible systematic variations due to different muon beam requirements, although this was not practical for the highest density sample.

### 3. Measurement

#### 3.1. *MuSR*

Based on our experience with muonium emission from silica powder, the identification of silica aerogel from a longer list of potential alternative candidate material samples was accomplished using the method of muonium spin rotation and relaxation (MuSR). The key properties that could be identified were: (1) a high probability for polarized muonium formation, similar to powder ( $0.64 \pm 0.03$  [13]), (2) low depolarization, or long persistence of the MuSR signal during the muon lifetime, and (3) an indication that Mu exits the fundamental structures of the material, signified by a distinctive increase in depolarization of the MuSR signal when oxygen is present in the target. The latter situation results from spin exchange interactions of muonium with paramagnetic oxygen molecules, which have been observed using gas [14] and silica powder [10, 15] as muonium-producing moderators. In addition to the aerogel slab samples as described in the previous section, the list of materials investigated included porous forms of silica and alumina, commercially available particulate aerogel (Nanogel) and silica powder (Cab-O-Sil) from Cabot Corporation [16], and a silica plate for calibrations and comparisons. Porous silica showed a relatively small MuSR muonium formation probability ( $0.21 \pm 0.01$ ), but it was unaffected by the introduction of oxygen, while alumina showed no significant signal even in vacuum. Silica powder and particulate aerogel samples both produced significant polarized Mu that showed depolarization with the introduction of oxygen, but because they are not self-supporting they were not investigated further except as a demonstration of the oxygen depolarization technique.

Based on muonium and muon asymmetries in MuSR measurements, the fraction of muonium formed in the three aerogel samples was  $0.52 \pm 0.01$ . The MuSR relaxation rate was of order  $0.05 \mu\text{s}^{-1}$ , indicating long-lived muonium polarization. The relaxation rate increased with the addition of oxygen into the sample environment at a rate proportional to the oxygen concentration and approximately consistent with comparable results for muonium in gas moderators [14] as well as for earlier silica powder moderators [10]. The decay time distributions were fit to oscillations of polarized muonium in an applied transverse magnetic field of 0.6 mT, as shown in Fig. 1. The apparent non-flat background is due to the much

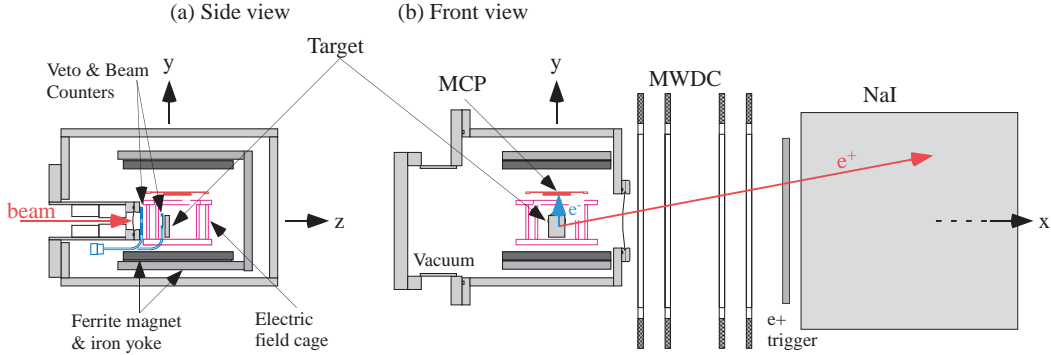


**Fig. 2** Setup for the muonium imaging measurement at the TRIUMF M15 beamline. The axes of the coordinate system  $(x, y, z)$  are indicated in the figure.

slower muon spin rotation signal. For high oxygen concentrations, the signal disappeared very quickly, indicating that nearly 100% of muonium in these aerogel samples was interacting with oxygen in the voids between the aerogel structure prior to muonium decay.

Note that while observation of this oxygen interaction is considered necessary for emission of muonium into a vacuum region separated from the moderating material, it is not sufficient. Useful production of muonium in vacuum for  $(g-2)_\mu$  must be established by identification of  $\mu$  in a region where it could be ionized by lasers, for example by the study of spatial and time distributions of muon (muonium) decay.

### 3.2. Space-time distribution of $\mu$

**3.2.1. Experimental Setup.** In order to measure the spatial and time distribution of muon decay, a dedicated setup (Fig. 2) was built at the end of the M15 surface muon channel at TRIUMF. Here the coordinate system  $(x, y, z)$  is defined as follows. The  $z$ -axis is along the beam center with the origin  $z = 0$  at the downstream surface of the target,  $y$  is in the vertical direction, and  $x$  is horizontal in the direction of the positron detection system. The measurement principle basically follows the previous experiments for silica powders [9, 11, 17], where the positron track was traced back to the plane bisecting the sample to calculate the position of muon decay.

The selected aerogel sample was placed in the vacuum chamber with the longer dimension vertical and with its downstream surface location fixed irrespective of the sample thickness. Muons passed the 10 mm hole in the veto scintillator and then through the 300  $\mu\text{m}$  thick beam scintillation counter before entering the target. Muons of the lowest practical momentum, typically  $\sim 23 \text{ MeV}/c$  (“subsurface” muons), therefore with the lowest spread  $\Delta p$  in momentum for fixed  $\Delta p/p$ , were used to increase the fraction of the muon beam that stops in a thin layer, thus reducing background from muons stopping elsewhere. For each target, a scan of beam momentum was performed. For each momentum in the scan, the number of muon decays observed from the target was normalized to the number of muons entering the target region. After corrections for dead time and rate effects, the result was compared with a simulation to obtain the fraction of the beam stopping in the target as the central momentum was varied. A flat-topped Gaussian-smear beam momentum distribution was used as input, where the flat top width and the smearing width at low and high momentum

---

ends were set common to all samples. The best values of the flat top width and smearing width describing the momentum scan data were 5% and 1.5%, respectively, relative to the central momentum. The central beam momentum was obtained independently for each target. This allowed a test of the simulated beam properties, and provided constraints for muon beam stopping distributions in each target. The beam momentum was then adjusted for each target so that approximately half of the incoming muons were stopped in the target, while the remainder passed through mostly to regions beyond those of interest for muonium decay in vacuum. This adjustment served to maximize the muon stopping density near the target surface at the downstream edge, nearest the vacuum decay region. Due to the similarity of the aerogel target masses, only small changes were necessary to find the optimum momenta (22.9, 23.2, 23.1 and 24.5 MeV/c, respectively). Thus systematic effects due to differences in muon momentum were significantly reduced.

Multi-wire drift chambers (MWDC) and a NaI detector were used to register positrons from muon decay and a micro-channel plate (MCP) detector was used to register electrons following muon decay in the muonium. The MWDC planes and readout electronics were previously used in the TWIST experiment at TRIUMF [18]. Four pairs of wire planes were used, with perpendicular planes in each pair. Each plane was 4 mm thick, with 80 wires at 4 mm intervals. The coordinates of hit wires were extrapolated to the plane containing the beam and target axis to provide a two-dimensional distribution of muon decay locations in and near the target. Since the thermal velocity of muonium in vacuum is of the order of 5 mm/ $\mu$ s and the time duration is of the order of the muon lifetime (2.2  $\mu$ s), we needed a positional resolution of a few mm or less. The intrinsic positional resolution of the MWDC is 0.2 mm or better, however the multiple scattering of positrons and the parallax effect of the extrapolation actually limited the tracking resolution. The NaI detector was used to select only high energy positrons ( $> 30$  MeV/c), reducing the effect of scattering.

Although the position sensitive multichannel plate (RoentDek HEX40 MCP) used to detect the low energy electrons that remain when the muon in muonium decays did sharpen the event-by-event position of the muonium decays (and distinguish events in vacuum from those in the aerogel), we have not yet determined the efficiency uncertainties of the MCP, precluding its use in this quantitative analysis.

*3.2.2. Extraction of space-time distribution.* A positron track was reconstructed by fitting a straight line to hit coordinates in the MWDCs. The confidence level of the fit was required to be greater than 95% to ensure good quality of reconstruction. A fiducial region was defined so that the positron track projection to  $x = 0$  lay within  $\pm 20$  mm in the vertical direction. A cut on track slope,  $|\frac{dz}{dx}| < 0.1$ , was applied to reduce the parallax uncertainty in the extrapolation. Because low energy positrons show larger multiple scattering angles, they were rejected by requiring deposited energy in the NaI to be greater than 30 MeV.

Reconstructed tracks were extrapolated back to the target area ( $x = 0$  mm) with an accuracy estimated as 2 mm ( $\sigma$ ) by a GEANT-based Monte Carlo simulation [19]. This was confirmed using the experimental data taken with a solid silica plate of 0.1 mm thickness that was used for calibration and background estimation.

The time of muon decay was measured as the time of positron detection in a pair of scintillators located behind the MWDCs, with respect to the beam counter. Corrections for slewing effects and light propagation in the scintillator were applied by using information on the

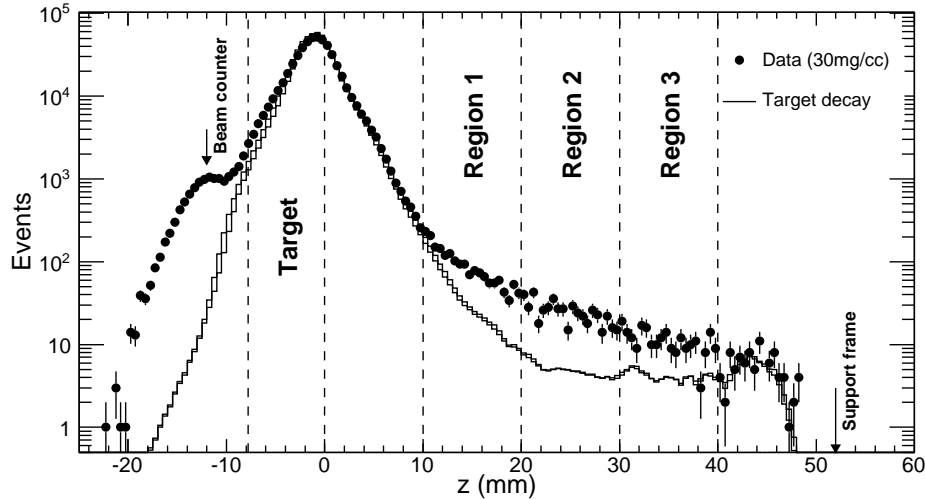


**Fig. 3** Distribution of positron track extrapolation positions. Closed circles shows data with  $29 \text{ mg cm}^{-3}$  aerogel. The histogram indicates the target decay distribution estimated from a simulation of muon stopping smeared by the extrapolation resolution.

pulse height of hits and reconstructed track position on the scintillator. The time resolution was estimated as  $1 \text{ ns}$  ( $\sigma$ ) from prompt positrons in the incoming beam scattered from the target and hitting the scintillators. The time distribution of positrons showed a prompt peak due to the prompt beam positrons followed by positrons from muon and muonium decay. The latter contributions were confirmed by the characteristic spectrum shape determined by decay lifetime and oscillation of yield due to muon and muonium spin rotation in the transverse magnetic field. The prompt beam positrons were eliminated in the following analysis.

The two-dimensional track extrapolation position distribution projected along the beam direction consists of three components. The first, which is dominant in the distribution, comes from positrons from muon or muonium decay in the target (target decay). The second is due to positrons from muonium decay in vacuum (vacuum decay). The third, due to positrons from decays in other locations such as the support structure or vacuum chamber walls, became negligible after applying fiducial volume selections.

The extrapolated spatial distribution for positrons from target decay is described by the convolution of the muon stopping distribution in the target and the extrapolation resolution. The muon stopping distribution was estimated with a Monte Carlo simulation by comparison with the measured stopping rate in the target as a function of beam momentum for each target density and thickness. The extrapolated distribution measured with the calibration target was used to characterize extrapolation resolution. Figure 3 shows the distribution of extrapolated position and the estimated contribution from the target-decay positrons. The total number of positron tracks in the region from  $z = -8.4 \text{ mm}$  to  $40 \text{ mm}$  was used to normalize the target-decay distribution to the number of muons stopping in the aerogel target. This normalization is then independent of the track reconstruction efficiency.

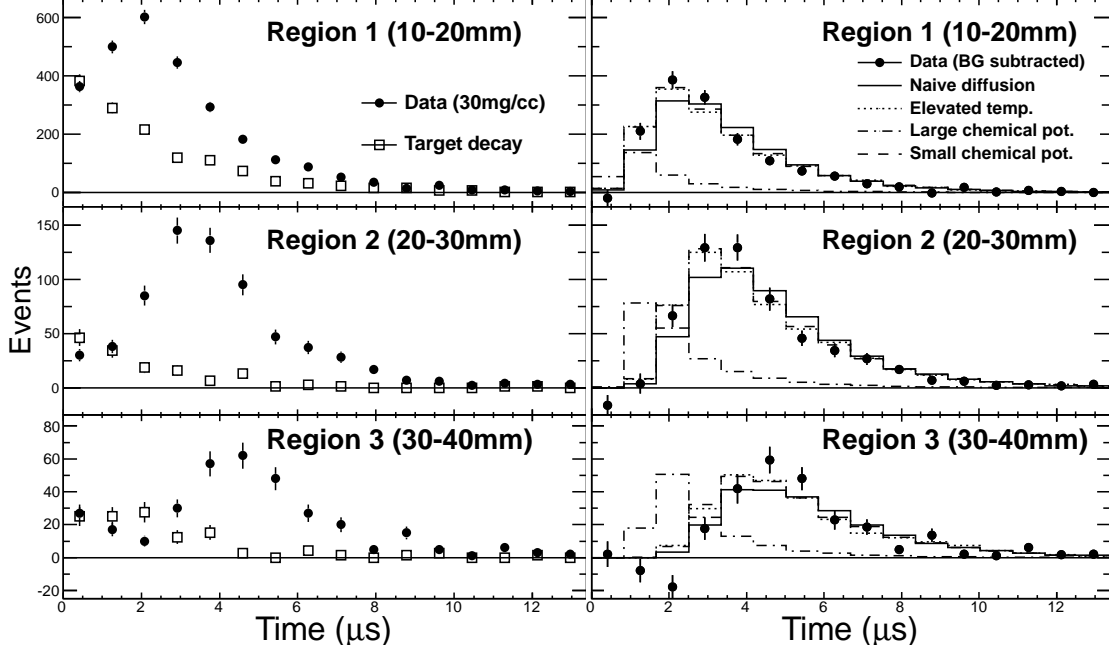


**Fig. 4** Left plots are time distributions of positrons in each region for  $29 \text{ mg cm}^{-3}$  aerogel. Right plots are background-subtracted time distributions compared with diffusion models.

Positrons from target decay are a dominant contribution near the target surface region, whereas there is an excess over the target-decay positrons in the vacuum region ( $z > 10 \text{ mm}$ ). The time structure of the excess events was examined by dividing the positron tracks into three  $z$  regions. We define the regions 1, 2, and 3 as  $10 < z < 20 \text{ mm}$ ,  $20 < z < 30 \text{ mm}$ , and  $30 < z < 40 \text{ mm}$ , respectively. The time distribution of each region is shown in Fig. 4 for the  $29 \text{ mg cm}^{-3}$  aerogel. In the plots in the left panel, data are shown as closed circles, and the target-decay events are shown as open squares. The target-decay events were estimated from data with the calibration target scaled by a normalization factor that was pre-determined in the comparison of the  $z$ -distribution (Fig. 3). The time distribution of the excess over the target-decay events has a peak that moves to later time as the selected region moves farther from the target surface.

The time distributions after subtracting for the target decay events were compared with models of muonium diffusion. The solid histograms in the right panel of Fig. 4 indicate predictions from three-dimensional diffusion at room temperature (naive diffusion model). In this model, muonium moves with velocity selected from a Maxwell distribution from its initial position and diffuses among silica grains until it decays or is emitted from the target surface. A parameter in this model is the mean free path between collisions. The angular distribution of muonium emission that naturally emerges from the target surface is approximately proportional to  $\cos \theta$ , where  $\theta$  is the polar angle of muonium with respect to the normal to the surface. The naive diffusion model describes basic features of the peaking structure in time and its evolution with spatial region. However, it underestimates data points at early time in region 1 and region 2, which correspond to fast-moving muonium.

**Table 1** Vacuum yield in the region 1–3 and mean free path

Density (mg cm <sup>-3</sup> )	Vacuum yield (per 1000 muon stops)	Mean free path ( $\mu\text{m}$ ) (small chemical potential model)
29	$2.74 \pm 0.11^{+0.10}_{-0.13}$	$0.226 \pm 0.016^{+0.113}_{-0.079}$
47	$2.81 \pm 0.11^{+0.14}_{-0.08}$	$0.118 \pm 0.009^{+0.060}_{-0.034}$
97	$3.13 \pm 0.20^{+0.12}_{-0.09}$	$0.035 \pm 0.004^{+0.018}_{-0.012}$
178	$1.60 \pm 0.11^{+0.07}_{-0.10}$	$0.0050 \pm 0.0007^{+0.0020}_{-0.0014}$

Three alternative models were considered to understand the early-time enhancement compared to naive diffusion. First, we consider that muonium is locally heated up when it is formed. Dotted histograms indicate the diffusion model with the initial temperature elevated to 400 K. Another possibility is that the initial muonium energy is elevated by a chemical potential as it exits a silica surface within the aerogel sample. Interpretation of muonium emission to vacuum with a chemical potential as large as 0.3 eV was reported for data taken with a mesoporous silica film [20]. We examined whether this could be present in these silica aerogels, with a simulation represented by dash-dotted histograms in Fig. 4. We found the simulated early-time enhancement is too large to explain the data for such a large chemical potential (0.3 eV). However, such a scenario may describe the data if the chemical potential is smaller (25 meV) and muonium energy is thermally moderated during the diffusion process (small chemical potential model). This model is shown as the dashed histograms in Fig. 4. The early-time data points are now better described by either the elevated-temperature or the small chemical-potential models.

The yield of muonium in the region 1–3 ( $10 < z < 40$  mm) per 1000 muons stopping in the aerogel was found to be  $2.74 \pm 0.11$ (stat.) $^{+0.10}_{-0.13}$ (syst.) for density 29 mg cm<sup>-3</sup>. This is based only on the background-subtracted data and is thus independent of the diffusion model. The mean free path in the diffusion model was estimated from the yield, assuming the muonium formation fraction of  $0.52 \pm 0.01$  as determined by MuSR. The mean free path is a model dependent quantity as it depends on the velocity distribution. The velocity distribution was not uniquely determined from the time distribution that is a convolution of muonium emission from aerogel and velocity. The value of the mean free path that best represents the time distributions varies by 10% among different models except the large chemical potential model. We obtained  $0.226 \pm 0.016$ (stat.) $^{+0.113}_{-0.079}$ (syst.)  $\mu\text{m}$  for density 29 mg cm<sup>-3</sup> using the small chemical potential model for the central value. The systematic uncertainties are dominated by the uncertainty of the muon beam momentum distribution, which is mostly correlated for all samples. Thus, this uncertainty is not relevant in the relative comparison of densities, except perhaps for the most dense sample. Note that the vacuum yields of the other three samples are approximately consistent within the stated uncertainties. However, comparison with simulations used central beam momenta and stopping distributions that were unique for each target, where small variations were important in assessment of mean free paths in the diffusion model for different densities of aerogel. The yields and mean free paths for all samples are given in Table 1



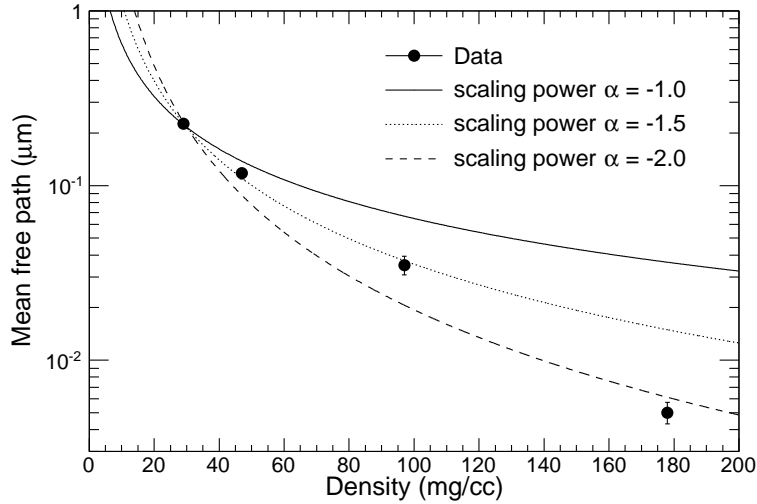


**Fig. 5** Mean free path and density of silica aerogel.

**Table 2** Specific surface area and estimated grain radius

Density ( $\text{mg cm}^{-3}$ )	Specific surface area ( $\text{m}^2 \text{g}^{-1}$ )	Estimated grain radius (nm)
29	550	2.5
47	620	2.2
97	716	1.9
178	914	1.5

Density dependence of the mean free path can be parameterized using a scaling power relation  $L = L_0(\frac{\rho}{\rho_0})^\alpha$  where  $\rho$  is the density,  $\rho_0$  and  $L_0$  are reference density ( $29 \text{ mg cm}^{-3}$ ) and its mean free path, and  $\alpha$  is a parameter. It is known that the muon stopping density (stopping muons per unit sample thickness) scales with the material density as  $\alpha_\mu = +1.0$ , i.e., there is a linear proportionality between stopping density and material density. The total yield in the vacuum region should scale as  $\alpha/2 + \alpha_\mu$  since the mean one-dimensional distance travelled in the diffusion process scales as  $\sqrt{L}$  for isotropic scattering. The value of  $\alpha$  is predicted to be  $-1.0$  in a simple geometric model that assumes silica aerogel consisting of grains of  $\text{SiO}_2$  spheres. In this case, higher yield is expected at higher density, but this gain with density would disappear if  $\alpha < -2.0$ . The density dependence of the mean free path is shown in Fig 5, where data are compared with three values of  $\alpha$ . The measured dependence is clearly larger than for  $\alpha = -1.0$ ; the dotted curve with  $\alpha = -1.5$  best describes the data, except for the  $178 \text{ mg cm}^{-3}$  aerogel. This would imply that the underlying mechanism for the density dependence is beyond the simple geometric picture.

The BET method [21] was used to estimate the specific surface area of all samples. The grain radius was estimated by assuming spherical shapes of  $\text{SiO}_2$  grains in the aerogel structure. They are shown in Table 2. It suggests that the grain size deduced from an assumption of  $\text{SiO}_2$  nano-spheres decreases with increasing sample density. Images from an electron-microscope (SEM/TEM) showed a grain-network structure, but the density dependence is

difficult to interpret and is not considered in this discussion. These microscopic differences may play an important role behind the observed density dependence.

#### 4. Discussion and prospects

For the comparison with the application of the  $g - 2$  experiment at J-PARC, the measured yield of vacuum emission needs to be scaled to match the beam conditions. According to the naive diffusion model discussed above, the total yield of Mu in vacuum  $y_{vac}$  from 29 mg cm<sup>-3</sup> is  $4.8 \times 10^{-3}$  per incident muon in a beam with a momentum spread of 2% (RMS) at 23 MeV/c. This includes those decaying outside of our measurement fiducial regions. The beam momentum and its spread at J-PARC is designed to be 28 MeV/c and 5% (RMS), respectively. Under the assumption that only a small region near the surface contributes to emission, the yield is proportional to the muon stopping density  $\rho_{stop}$  at the surface, which in turn is inversely proportional to the range spread  $\Delta R$  of the muon stopping distribution. For a surface muon beam, assuming the relatively small range straggling term [22] in the range spread can be ignored, the range spread is proportional to the total range  $R$ . Total range  $R$  scales with momentum as  $p^{3.5}$  with the proportionality constant depending on the the relative momentum spread of the beam  $\delta p = \frac{\Delta p}{p}$ . Therefore, the vacuum yield  $\tilde{y}_{vac}$  with other beam conditions is estimated from  $y_{vac}$  as

$$\tilde{y}_{vac} = \left( \frac{\tilde{\rho}_{stop}}{\rho_{stop}} \right) y_{vac} = \left( \frac{\Delta R}{\Delta \tilde{R}} \right) y_{vac} = \left( \frac{\delta p}{\delta \tilde{p}} \right) \left( \frac{p}{\tilde{p}} \right)^{3.5} y_{vac}, \quad (1)$$

where variables with a tilde indicate conditions to be estimated. In the case of J-PARC beam conditions, we obtained  $\tilde{y}_{vac} = 9.6 \times 10^{-4}$ .

The probability of muonium emission to vacuum is calculated by using diffusion models with parameters estimated in this work. In the models, the probability drops exponentially as a function of distance of the initial muonium formation point from the surface. For 29 mg cm<sup>-3</sup> aerogel, the probability goes down to  $e^{-1}$  at 30  $\mu\text{m}$  from the surface in the small chemical potential model. On the other hand, the stopping distribution of incoming muons spreads over a few millimeters due to the energy loss and range straggling and the momentum width of the muon beam. Therefore the length scale of diffusion is much shorter than that of the stopping distribution. This is one of the major limitations to higher muonium production yield in vacuum. The consequence of this is that improvement of yield in vacuum might be anticipated if one introduces an intermediate structure which is porous or has peaks and valleys of 100  $\mu\text{m}$  in scale so that muonium may reach the surface promptly during the diffusion process before decay. Development of such a silica aerogel sample will be the subject for future research to increase the yield.

#### 5. Conclusions

Muonium emission from several silica aerogel samples of different densities was confirmed in this work. The space-time distribution of muonium follows a naive diffusion model. Some possible deviations from this naive diffusion model in the early part of the time spectrum are observed. The density dependence of the mean free path is weaker than predicted by naive scaling, and there is no strong enhancement of the yield at higher densities. There is potential for an increase of the production yield by introduction of intermediate structure having a scale of approximately 100  $\mu\text{m}$ .

---

## Acknowledgements

The authors are pleased to acknowledge the support from TRIUMF to provide a stable beam during the experiment. Special thanks go to R. Henderson, R. Openshaw, G. Sheffer, and M. Goyette from the TRIUMF Detector Facility. We also thank D. Arseneau, G. Morris, B. Hitti, R. Abasalti, and D. Vyas of the TRIUMF Materials and Molecular Science Facility. Research was supported in part by the MEXT KAKENHI Grant Number 231800N (Japan) and NSERC Discovery Grant (Canada).

## References

- [1] T. Nagae (ed), Prog. Theor. Exp. Phys. (2012), Special issue 2.
- [2] G.W. Bennett et al., Phys. Rev. D **73**, 072003 (2006).
- [3] K. Hagiwara, R. Liao, A.D. Martin, D. Nomura, and T. Teubner, J. Phys. G **38**, 085003 (2011).
- [4] M. Davier et al., Eur. Phys. J. C **71**, 1515 (2011), Erratum-ibid. **72**, 1874 (2012).
- [5] J.H. Brewer, K.M. Crowe, F.N. Gygax, and A. Schenck, Positive Muons and Muonium in Matter, in *Muon Physics Vol. III*, eds. V.W. Hughes and C.S. Wu, (Academic press, New York, 1975), pp 4-140.
- [6] L. Willman et al., Phys. Rev. Lett. **82**, 49 (1999).
- [7] S. Chu et al., Phys. Rev. Lett. **60**, 101 (1988).
- [8] V. Meyer et al., Phys. Rev. Lett. **84**, 1136 (2000).
- [9] G.A. Beer et al., Phys. Rev. Lett. **57**, 671 (1986).
- [10] G.M. Marshall et al., Phys. Lett. A **65**, 351 (1978).
- [11] K.A. Woodle et al., Z. Phys. D **9**, 59 (1988).
- [12] M. Tabata et al., Nucl. Instrum. Meth. A **668**, 64 (2012).
- [13] R.F. Kiefl et al., Hyp. Int. **6**, 1857 (1979).
- [14] M. Senba, D.G. Fleming, D.J. Arseneau, D.M. Garner, and I.D. Reid., Phys. Rev. A **39**, 3871 (1989).
- [15] J.R. Kempton et al., Hyp. Int. **65**, 811 (1990).
- [16] Cabot Corporation, 157 Concord Road, Billerica, MA 01821, USA.
- [17] A.C. Janissen et al., Phys. Rev. A **42**, 161 (1990).
- [18] R.S. Henderson et al., Nucl. Instrum. Meth. A **548** 306 (2005).
- [19] <http://geant4.cern.ch>
- [20] A. Antognini, et al., Phys. Rev. Lett. **108**, 143401 (2012).
- [21] S. Brunauer, P.H. Emmett, and E. Teller, J. Am. Chem. Soc. **60**, 309 (1938).
- [22] A.E. Pifer, T. Bowen and K.R. Kendall, Nucl. Instrum. Meth. **135**, 39 (1976).